Nanoscale

Accepted Manuscript

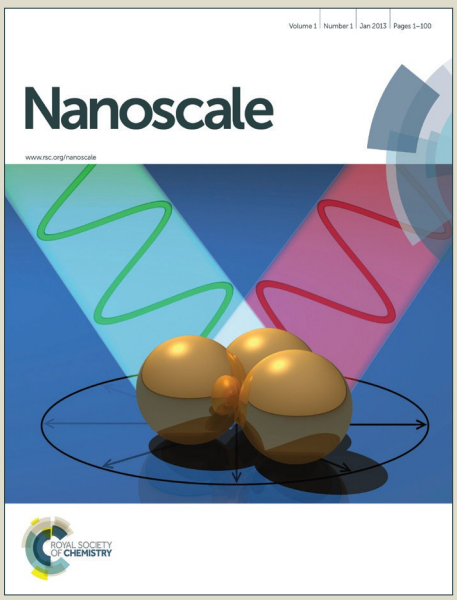

ROYAL SOCIETY OF CHEMISTRY

www.rsc.org/nanoscale

Journal Name

ARTICLE

Chirality-dependent densities of carbon nanotubes by in situ 2D fluorescence-excitation and Raman characterisation in a density gradient after ultracentrifugation.

Received 00th January 20xx,
Accepted 00th January 20xx

Sofie Cambré, Pieter Muyshondt, Remi Federicci and Wim Wenseleers *

DOI: 10.1039/x0xx00000x

www.rsc.org/

Density gradient ultracentrifugation (DGU) becomes increasingly important for the sorting of nanomaterials according to the particles' density, hence structure and dimensions, which determine their unique properties, but the further development of this separation technique is hindered by the limited precision with which the densities could be characterized. In this work, we determine these densities by position-dependent 2D wavelength-dependent fluorescence-excitation and resonant Raman spectroscopy measured directly in the density gradient after ultracentrifugation. We apply this method to study the diameter and chirality-dependent sorting of empty and water-filled single-walled carbon nanotubes coated with two different surfactants, sodium cholate (SC) and sodium deoxycholate (DOC). The results elucidate the long standing contradiction that SC would provide better diameter sorting, while DOC is the most efficient surfactant to solubilise the nanotubes. A more predictable separation is obtained for empty DOC-coated nanotubes since their density is found to vary very smoothly with diameter. The accurate and chirality-dependent densities furthermore provide information on the surfactant coating, which is also important for other separation techniques, and allow to determine the mass percentage of water encapsulated inside the nanotubes.

Introduction

The unique and remarkably diverse electronic and optical properties of nanomaterials depend critically on their specific size and shape, even if their chemical structure is very similar.[1-3] A well-known prototypical example are single-walled carbon nanotubes (SWCNTs),[2, 4] consisting of a rolled-up graphene sheet with diameters of 0.5nm up to a few nm and typical lengths of a few microns. Their electronic and optical properties are critically dependent on their exact diameter and chiral structure (uniquely described by the chiral indices (*n*,*m*) of the so-called roll-up vector of the graphene sheet).[2] The lack of control in their synthesis, producing inhomogeneous mixtures of different diameters/chiralities, band gaps, etc., has created a huge need for specialized separation and purification methods, as well as dedicated characterization methods to distinguish species based on their structure and size dependent properties.

While originally developed for the separation of bio- and other macromolecules[5], in recent years density gradient ultracentrifugation (DGU) is booming as a very versatile and generally applicable tool for nanomaterials research.[6] Particles with different size or shape can be separated based on their different sedimentation rate (i.e. rate zonal ultracentrifugation), and/or based on their difference in buoyant density in isopycnic DGU.[8] The buoyant density, the key parameter for these isopycnic separations, not only depends on the exact size and shape of the nanomaterials, but also on the structure of the adsorbed dispersant layer.

Since the pioneering work of the Hersam group[6], DGU has emerged as one of the most widely used and versatile techniques for the sorting of CNTs by diameter/chirality[6, 10], length[11], electronic structure[6], number of walls[12], filling state[13, 14], and even enantiomers can be separated.[15] Pure solutions (>99%) of semiconducting or metallic tubes are already commercially available and single-chirality dispersions are achievable at laboratory scale for particular chiralities.[10] DGU has furthermore shown to be efficient for the sorting of graphene and other 2D materials according to the number of layers[7, 16] and the sorting of metallic nanoparticles according to their specific size.[8, 9]

In spite of these very nice demonstrations of the separation of carbon nanotubes (and other nanomaterials), the separation mechanisms are not yet well understood, and various parameters are not yet optimised, which makes it impossible to predict and control the separations.

Analytical ultracentrifugation (AUC) could be very helpful in this perspective;[9, 17, 18] but analytical ultracentrifuges are limited to UV-VIS spectroscopy and refractive index

[a] *Experimental Condensed Matter Physics Laboratory, Physics Department, University of Antwerp, Antwerp, Belgium; E-mail: Wim.Wenseleers@uantwerpen.be*

Electronic Supplementary Information (ESI) available: (1) density calibration, (2) fraction selection and reproducibility, (3) diffusion of the SWCNTs and (4) experimental RRS spectra and fits at various excitation wavelengths. See DOI: 10.1039/x0xx00000x

measurements, which is insufficiently selective to distinguish individual CNT species in a polydisperse sample. A tedious workaround for this problem has recently been proposed, by first obtaining length-sorted single-chirality (6,5) solutions and using these as starting point for the analytical centrifugation,[18] thus, however, only yielding the density of one single chirality at a time. It is of course much more important to understand and control the differences in densities between different chiralities, as these determine the possibility to separate SWCNT chiralities (or other nanomaterials) from each other.

We have previously obtained such information, i.e. buoyant density as a function of SWCNT diameter and chiral structure, by manually selecting different fractions from the centrifuge tube and measuring extensive wavelength-dependent resonant Raman (RRS) and fluorescence-excitation (PLE) spectra of these separated fractions.[13] Such measurements are however extremely time consuming, too, and result in large error bars on the density determination due to the minimal volume of the discrete, manually selected fractions. General trends of the density - diameter relation could be obtained, but, to determine, understand and eventually control the density of different chiralities, a higher density-resolution is indispensible.

Ghosh *et al*.[10] proposed to perform fluorescence experiments (with a single laser excitation) as a function of height, *in situ* in the centrifuge tube, immediately after centrifugation, thus directly obtaining the density variation for a small subset of SWCNTs (those in resonance with the laser excitation). In this work, we show that the full position-dependent composition of the centrifuge tube after DGU can be characterized by the combination of a dedicated ultrasensitive wavelength-dependent IR fluorescence-excitation (PLE) and a resonant Raman scattering (RRS) spectrometer, both equipped with an automated translation stage.

We demonstrate the efficiency and importance of this new method, by comparing two well-known surfactants, sodium cholate (SC) and sodium deoxycholate (DOC) in their ability to sort SWCNTs by diameter. Previously, we have found that both of these bile salt surfactants are extremely efficient in solubilising SWCNTs[19], without the use of sonication, therefore resulting in a high concentration of individually isolated intact SWCNTs in solution. These surfactants furthermore provide a very homogeneous, non-perturbing surrounding for the SWCNTs, as exemplified by the high resolution in optical spectroscopy and the long-term stability of the solutions (>10 years). While only distinct in one hydroxyl-group, these surfactants have been shown to behave quite differently in DGU separations. While DOC provides a better solubilisation,[19] the best DGU chirality separations are surprisingly obtained with SC.[6, 10, 13, 20] The *in situ* characterisation helps in elucidating this long-standing contradiction.

Experimental Details

Sample preparation:

Sodium deoxycholate (DOC, also referred to as SDC in the literature, 99%) and sodium cholate (SC, 99%) were purchased from Acros organics. Raw SWCNTs from two different synthesis methods, high Pressure CO conversion[21] (HiPco from CNI, batch R0495C) and arc-discharge synthesis[22] (ARC from Nanoledge, batch P00508D) with typical lengths of the original raw material ranging from ~100-1000nm (suppliers specifications), were solubilized (10mg/3mL) in a 1%wt/V surfactant solution in D_2O (Cortecnet, 99.89%), using only gentle stirring for 3 weeks (no sonication, as sonication would result in a much larger fraction of opened and thus water-filled SWCNTs[23]).

The so-obtained solutions were centrifuged for 24 hours at 16215g (Sigma 2-16KCH centrifuge with swing-out rotor, 14000rpm), and the supernatant was collected for further sorting. This first medium speed 'pre-centrifugation' is based on sedimentation rate rather than density, to sediment out nanotube aggregates and bundles and end up with individually isolated SWCNTs in solution, and is particularly useful for the *in situ* experiments, where background absorption due to such impurities would otherwise limit signal strengths.

The density gradient medium used throughout this study is iohexol (tradename 'NycoDenz', obtained from Axis-shield as powder form), a monomeric analogue of the more commonly used dimer iodixanol.[6] While similar densities can be achieved, the lower molecular weight of iohexol makes it less sensitive to redistribution under the influence of the centrifugal field – a common limitation in maintaining shallow gradients during strong and/or prolonged ultracentrifugation. The higher density of D_2O allows the required density to be reached with lower mass-fractions of the gradient medium added, thereby further helping in creating more stable, shallow gradients.

Gradients were prepared in 1.3mL (30 mm height) thinwall polyallomer centrifuge tubes, which are transparent in the visible and NIR. Starting from a step gradient (low density layer (700µL of e.g. 1.15g/mL) added gently on top of a higher density layer (600µL of e.g. 1.27g/mL)), the centrifuge tube was tilted ~80° and rolled around its axis to form a continuous gradient. SWCNTs were added to both layers, to achieve a higher concentration for the *in situ* measurements. The density of both layers was slightly adapted between experiments to have the most important SWCNT bands located in the center part of the centrifuge tube (see below). The surfactant concentration in both layers of the step gradient was brought to 2%wt/V. We initially chose this relatively high surfactant concentration (also used in some previous work[13, 17, 24]) as a precaution to avoid reaggregation during centrifugation.

Centrifugation was performed at 20°C, for 48h at 28.000rpm (122.000g max) using a swing-out rotor (Kontron Centrikon T-1080, rotor TST 28). Visually no difference could be observed between 24h and 48h centrifugation runs, therefore we chose 48h centrifugation times to be sure that the SWCNTs have reached their isopycnic point within very close approximation.

Experimental Setups:

Absorption spectra were collected using a Varian Cary 5E UV-VIS-IR spectrometer in the range of 200-2500nm, using a quartz microcell (60µL) with a path length of 3mm. The densities were determined by calibration of a specific vibrational overtone absorption peak of iohexol, at 2285nm, against iohexol solutions of known concentration and density (determined using a pycnometer) and corrected for small amounts of H_2O in D_2O (see Supplementary Information (SI) Figures S1 and S3).

Raman spectra were recorded in backscattering geometry using a Dilor XY800 triple spectrometer with liquid nitrogen cooled CCD detection. Several excitation wavelengths from different laser systems (Ar^+, Kr^+, tuneable Ti:sapphire lasers from Spectra-Physics models 2020, 2060 and 3900S, respectively) were used for resonant excitation in the optical transitions of different SWCNTs.

In order to obtain a high sensitivity over the full emission wavelength range of the SWCNTs, a high power pulsed Xe-lamp excitation (Edinburgh Instruments, custom adapted Xe900/XP920) was combined with a liquid-nitrogen cooled extended InGaAs photodiode array detector (Princeton Instruments OMAV:1024/LN-2.2), sensitive up to 2.2µm. Spectra were corrected for detector and spectrograph efficiency, emission filter transparency, and (temporal and spectral) variations of the excitation light intensity using a reference detector measuring the intensity of each lamp pulse. *In situ* experiments were performed by mounting an automated translation stage in the sample chamber of the Raman and PLE setups. A horizontal strip of excitation light was achieved by using a cylindrical lens (in RRS) or by exploiting the combination of a horizontal image of the excitation spectrometer slit with a limited probe volume determined by the emission spectrometer slit (in PLE).

A single 2D PLE map was acquired in 10-15 min, with 5nm excitation wavelength steps (~60 different excitation wavelengths per map) and an instrumental resolution of ~8nm in excitation and ~15nm in emission wavelength, resulting in a spatial resolution of 230µm. Typical 1D RRS spectra (single excitation wavelength) were acquired in ~1-5min, with sub-wavenumber spectral resolution and a spatial resolution of ~200µm. Typically, the 2D+1 PLE maps were acquired with 1mm steps in height, while the 1D+1 RRS spectra were acquired with 0.1 or 0.5mm steps (where the +1 indicates the height dimension); and the height range was adjusted for each experiment taking into account that measurements needed to be performed before significant diffusion takes place. However, due to the large aspect ratio of SWCNTs, diffusion is quite slow as exemplified in Figure S4, SI. Within the typical 6-10 hour time-frame after DGU necessary to complete all experiments on one sample (strongly depending on the specific range of excitation wavelengths), a maximum error in density of only 0.002g/mL can be expected.

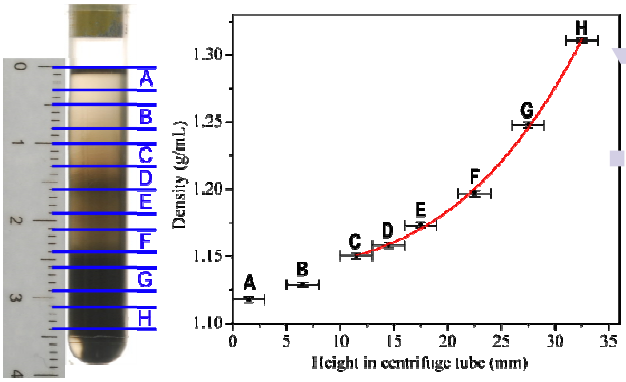

Fig. 1 Photograph of a centrifuge tube (left) containing a mixture of ARC and HiPco SWCNTs (2%DOC) after centrifugation for 48h at 122.000g. The selected fractions a e indicated on the photograph, resulting in the density-profile shown on the right. Tl red curve represents a polynomial fit to the acquired data within the range of the i situ experiments. Fractions A and B don't contain any SWCNTs and are therefore n t included in the fit. Fraction H contains mainly bundles of SWCNTs.

Density Calibration:

To be able to determine the density of the SWCNTs after isopycnic DGU, the height in the centrifuge tube needs to b calibrated to the respective density. Typically, for each DG run, 3-4 identical samples were prepared, so that RRS and PLE experiments could be acquired at the same time, i.e. in different centrifuge tubes; and from the other 1-2 samples we manually extracted well-defined 60-80µL (~3mm height) fractions using a syringe, to determine the density profile in the centrifuge tubes. Fractions were collected immediately after the DGU run, before diffusion of the gradient mediu (which occurs much faster than diffusion of the nanotubes). The fractions were selected with 1-2 mm spacing betwee them, so that mixing with higher or lower density layers could be avoided (Fig. 1).

The density of the fractions was determined using the absorption of iohexol in the NIR (see SI, Figure S1). Wh comparing the density profiles in two different centrifuge tubes of the same run, densities can be accurately reproduced in the central height range (5 to 25 mm; error < 0.002g/mL see Figure S3), while for the top and bottom of the centrifug tube the density varies much more steeply and larger deviations between different centrifuge tubes are obtained, of the order of 0.002-0.007g/mL. Density ranges were therefor chosen in such a way that the most important SWCNT layer end up in this central height range. Figure 1 presents a typic density-profile within the centrifuge tube after DGU. The data is fitted in the relevant height range using a polynomial.

To increase the diameter-range that can be studied in a single experiment, we mixed arc-discharge SWCNTs (d=1.0-1.5nm) and HiPco (d=0.6-1.2nm) solutions before the DGU-run. The density range was also chosen so that both empty and water-filled tubes,[13] of all these different chiralities, end up within the appropriate part of the centrifuge tube, where the accuracy of the density determination is the highest. Note that because of this broad diameter distribution (and steep gradient hence required), it is not possible to visually ass

the diameter separation by the appearance of colours in the centrifuge tube (Fig. 1), but spectroscopically all chiralities can still be distinguished in this mixed sample.

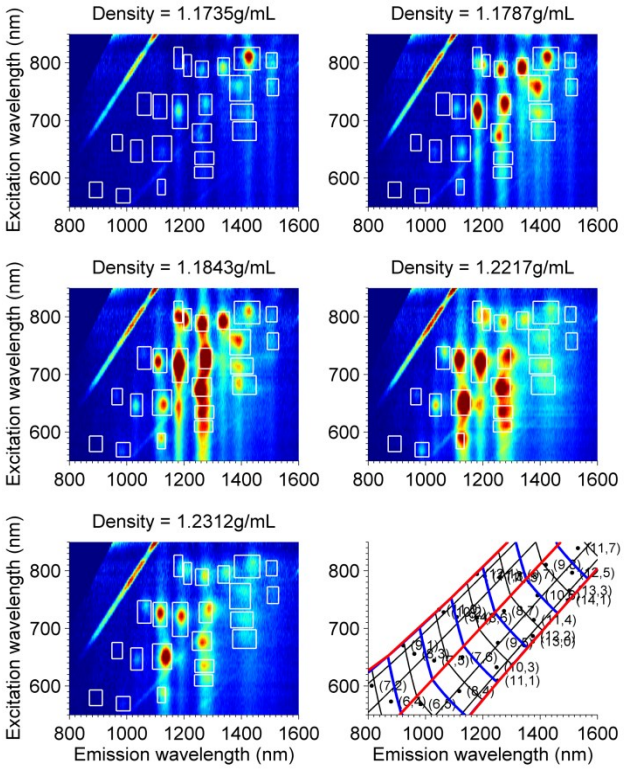

Fig. 2 Extracts from the 3D dataset, showing PLE plots obtained at different heights in the centrifuge tube. The white squares indicate the positions of the different chiralities, and the respective integration regions for obtaining their density profile (see text). The bottom right panel shows the diameter-chiral angle grid, with the red lines corresponding to lines of equal chiral angle (middle = chiral angle 0º and two outer lines are chiral angle 30º, with steps of 10º) and the blue lines are lines of constant diameter, with the spacing between the blue lines 0.1nm. Predicted peak positions of empty individual chiralities are also given.[13]

Results and discussion

PLE experiments

Figure 2 presents a selection of PLE maps acquired at different heights in the centrifuge tube. As such a 3D dataset is obtained, i.e. intensity as a function of emission wavelength, excitation wavelength and height (or density) in the centrifuge tube. To extract the diameter/chirality-selective information from this 3D dataset, one can proceed in different ways:

A direct overview of the density as a function of diameter can be obtained by using our previously developed method to project the PLE maps on a diameter axis.[13] Based on the empirical relations for the electronic transition energies of semiconducting SWCNTs as a function of diameter and chiral angle of the nanotubes (first put forward by Bachilo *et al.*[25] and further adapted for empty SWCNTs solubilised with DOC in reference [13]), a grid of lines of constant diameter and constant chiral angle (presented in the bottom right panel of Figure 2) can be obtained. The PLE spectra can then be integrated over strips of constant diameter, thereby reducing each 2D PLE maps to a 1D dataset: fluorescence intensity versus diameter. As such, the 2D+1 data set can be reduced to a 2D data set, as shown in Figure 3.

Typically two branches are observed, corresponding to the empty (lower density branch, E) and water-filled (higher density branch, F) SWCNTs, and it can be directly observed that the empty and filled tubes in general sort in the opposite order, i.e. with the empty tubes having lower densities for larger diameters, as we previously found in reference [13]. A clear difference between SC- and DOC-coated SWCNTs can be immediately observed, which will be discussed further on.

To obtain a more detailed, chirality-dependent analysis of the sorting of the SWCNTs, the PLE maps can also be integrated over a fixed excitation and emission interval (white boxes in Fig. 2), including only a single PLE-peak, corresponding to one specific chirality. For larger diameters, where the electronic shifts due to water-filling become much larger and signals

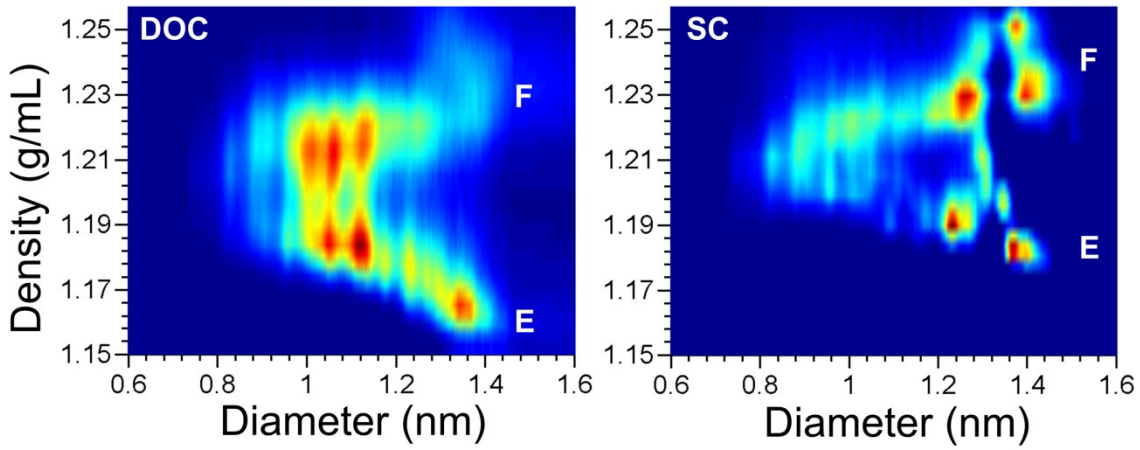

Fig. 3 Projection of the PLE maps on diameter, as a function of density in the centrifuge tube for 2%w/V DOC (left) and 2%w/V SC (right), combining the data acquired for HiPco and arc-discharge SWCNTs. Lower density branch corresponds to the empty tubes (E) and the upper density branch to the water-filled (F) carbon nanotubes.

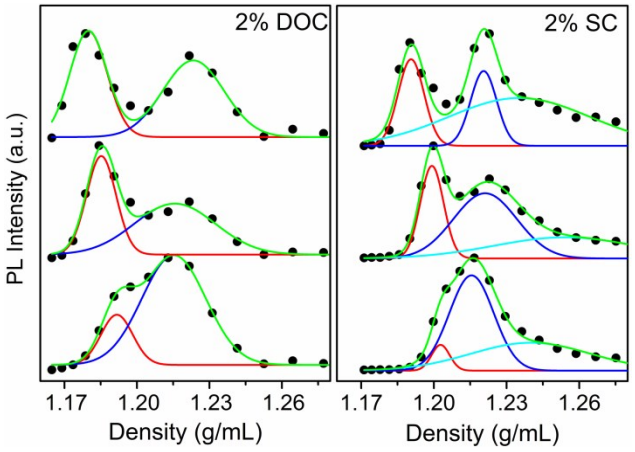

Fig. 4 PLE-intensity for different chiralities as a function of density in the centrifuge tube. From top to bottom: (9,8), (10,5) and (7,6). Fits are performed using a sum of Gaussians, corresponding to empty (red) and water-filled (blue) tubes. For the SC sample, due to the asymmetry of the bands, an additional Gaussian (cyan) is added to the fits, attributed to partially re-aggregated SWCNTs. An enlarged version can be found in the SI, Figure S2

filled tubes of one specific chirality might overlap with empty tubes of a different chirality, separate integration regions for empty and filled tubes were used. As such a 1D data set is obtained for each chirality, i.e. intensity versus density, a representative selection of which is shown in Figure 4.

When using DOC, two symmetric bands are observed for each chirality, corresponding to the empty (lower density) and water-filled (higher density) SWCNTs, which can each be fitted with a Gaussian. The bands remain resolved in density, even for relatively thin diameters (*e.g.* (7,6): *d*=0.88nm).

When using SC however, asymmetry in the bands is clearly observed, with a tail at higher density, most probably arising from partial reaggregation during the centrifugation. Large bundles can be found as a distinct band at much higher density. In Figure 4 we fitted this asymmetry by adding an additional Gaussian band to the curve, accounting for the partially aggregated SWCNTs. For the smallest diameters, the density profiles of empty and filled tubes (red and blue curves in Figure 4) strongly overlap and fitting results in large error bars on the determined densities. To solve this issue, we used RRS spectroscopy (see below).

Finally, the density profile of all the water-filled tubes is much broader than that of the empty tubes, which can be ascribed to the counteracting effects of gravity versus diffusion during the ultracentrifugation, where the pristine, empty and thus full-length SWCNTs will diffuse much less than the shorter, cut and therefore water-filled tubes.

RRS experiments

In addition to the PLE experiments, we also measure RRS spectra as a function of height in the centrifuge tube. With RRS only a subset of SWCNTs in resonance with the laser wavelength can be studied at a time, however also metallic SWCNTs can be studied and a higher spatial resolution can be achieved (laser vs. lamp excitation).

Figure 5 presents the RRS spectra obtained at a laser excitation of 647.1nm, in resonance with two ranges of SWCNTs, large diameter metallic and smaller diameter semiconducting SWCNTs. Due to the high sensitivity of the RBM vibration to (external and internal) environment of the SWCNTs,[9, 23, 26, 27] in combination with the high spectral resolution of the RRS spectrometer, the RBMs of empty and water-filled SWCNTs can be easily resolved spectrally, due to their shifted RBM vibration, and thus RRS allows obtaining the concentrations of

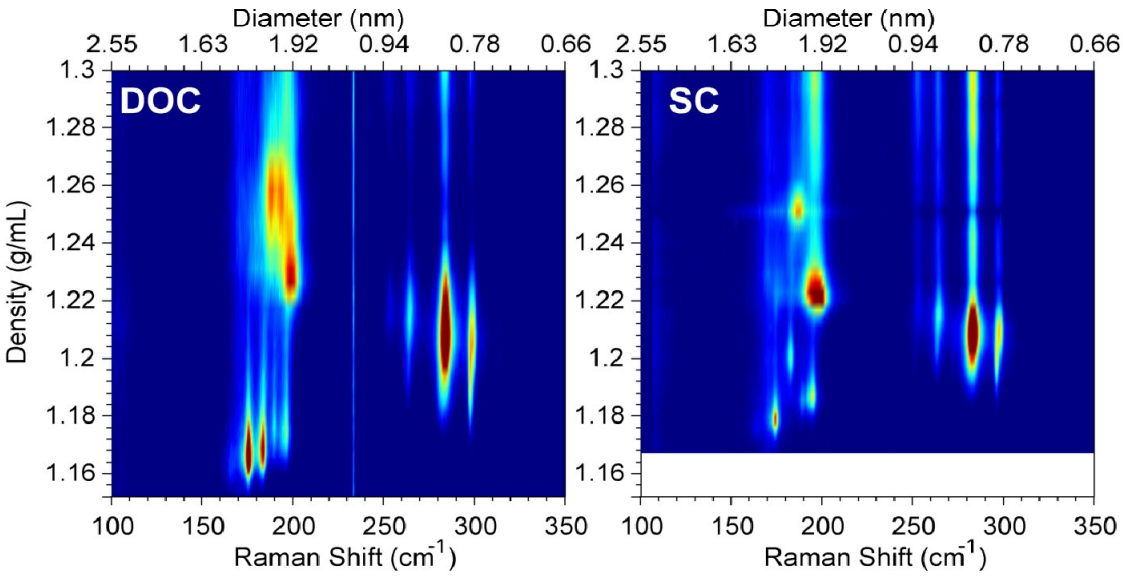

Fig. 5 RRS spectra excited at 647.1nm as a function of density (height) for 2% w/V DOC (left panel) and SC (right panel). The fits of these experimental data as well as the RRS spectra excited at other excitation wavelengths can be found in the SI. (Note that in contrast to Fig. 3, the diameter increases to the left in this figure).

Journal Name

ARTICLE

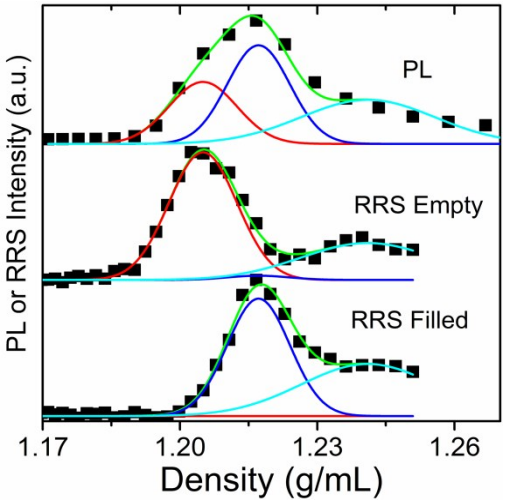

Fig. 6 Comparison of the density profiles of the (7,6) SWCNTs (2% SC) obtained from the PLE measurements (i.e. bimodal distribution of empty and filled SWCNTs) and from the fits of the RRS spectra where empty and filled SWCNTs can be spectrally separated. Fits (green) are superpositions of 3 Gaussians, corresponding to empty (red), water-filled (blue) and an additional band for small aggregates that are formed during the centrifugation with SC (cyan). The 3 data sets were fitted simultaneously to achieve a better determination of the peak positions and line widths.

empty and water-filled SWCNTs separately as a function of height in the centrifuge tube directly from the spectra, in contrast to the PLE experiments, where the position-dependent concentrations of empty and water-filled SWCNTs can only be determined by fitting the bimodal density-distribution. Since the RBMs of empty and water-filled SWCNTs partly overlap (shifts ~1-4cm-1) we fitted these 2D data sets using for each chirality two Lorentzians, corresponding to the empty and filled tubes, of which the line widths and peak positions are fitted simultaneously for all the different heights (densities), i.e. each spectrum is fitted with exactly the same line width and peak positions, only the amplitudes are allowed to vary (see Figures S5-S8). As such one obtains a very accurate determination of the RBM positions for the empty and the filled tubes, similarly as in previous work where different samples with different empty/filled compositions were fitted simultaneously.[23, 26] It should be stressed that for these fits, only the spectra with densities smaller than 1.27g/mL were selected, i.e. the density region of the isolated empty and filled tubes, thereby eliminating the densities where the bundles reside. These bundles have larger line widths than the individualized SWCNTs and are slightly red-shifted.[28] The advantage of spectrally resolving the empty and water-filled SWCNTs in RRS, is in particular important for the small diameter SWCNTs where the difference in density between empty and water-filled SWCNTs is very small. Figure 6 gives the comparison of the PLE and RRS density profiles of the (7,6) SWCNTs (2% SC), from which it is clear that RRS can be very helpful for a more accurate determination of the positions of empty and water-filled SWCNTs, if their density profiles partly overlap. In particular, by combining experiments and simultaneous fitting, the peak positions and line widths can be more accurately determined.

Combination of RRS and PLE

Far more precise than possible by manually extracting fractions, Figure 7 presents an overview of the densities for all

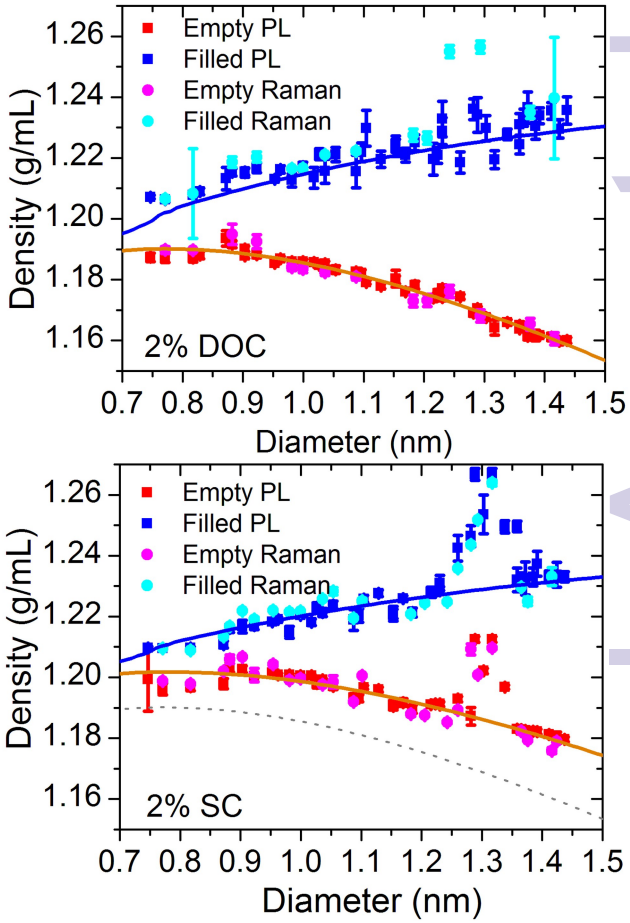

Fig. 7 Density versus diameter plots for empty (red, magenta) and water-filled (blue, cyan) SWCNTs obtained from PLE and RRS experiments, respectively. The orange solid lines represents a fit of the experimental data for the empty SWCNTs, using equation 1 and fitting the thickness and density of the surfactant layer. The blue curve is calculated using the same thickness and density of the surfactant layer, and assuming filling of the SWCNTs according to the hard sphere model from Picket et al.[29] and extended to larger diameters in [13] (see text). For comparison, the model curve for empty DOC-coated SWCNTs is repeated in the bottom panel (gray dashed curve).

empty and filled SWCNT chiralities observed, combining the RRS and PLE experiments for 2% w/V DOC and SC. Data points are from the individual fits of the PLE and RRS data, thus some of the semiconducting tubes are presented twice in this plot. In total, densities of 50 (51) different empty and water-filled chiralities for DOC (SC) respectively, were determined of which the density-diameter dependence will be modelled in the next section.

Modelling of the surfactant layer

Three main differences can be observed between DOC and SC-dispersed SWCNTs (Figure 7):

First of all, the densities of empty SC-wrapped SWCNTs are clearly higher than those of empty DOC-wrapped SWCNTs (both 2%w/V surfactant concentration ; the higher buoyant density of SC-wrapped than DOC-wrapped tubes is also in good agreement with the AUC data reported by Fagan *et al.* for (6,5) SWCNTs with 1% surfactant, see Fig. 7 in ref. [18]), and decrease less with diameter. To understand this difference, we introduce a simple geometric model for the buoyant density of SWCNTs (Fig. 8a), consisting of two concentric cylindrical shells, corresponding to the SWCNT wall and the surfactant-hydration layer surrounding the tube.[13, 30] The buoyant density of SWCNTs can then be calculated as $\rho = M_{total}/V_{total}$ where V_{total} and M_{total} are the total volume and mass per unit length and

$$V_{total} = \pi(d_{NT}+d_{wall}+2d_{surf})^2/4,$$
$$M_{total} = \pi/4\,[\rho_{int}\,(d_{NT} - d_{wall})^2 + \rho_{wall}\,((d_{NT} + d_{wall})^2 - (d_{NT} - d_{wall})^2) + \rho_{surf}\,((d_{NT} + d_{wall}+2d_{surf})^2 - (d_{NT} + d_{wall})^2)] \quad \text{(eq.1)}$$

with d_{NT} the diameter of the SWCNT, which we calculated using the widely accepted C-C distance of 0.142nm; d_{wall} and ρ_{wall} the thickness and density of the SWCNT wall, which we approximated by those of one graphite layer, i.e. d_{wall}=0.34nm and ρ_{wall}=2.23g/mL and ρ_{int} is the density of the SWCNT-cavity, which is either 0 for empty SWCNTs, or is determined by the density of the water inside the SWCNTs, which we will discuss later.

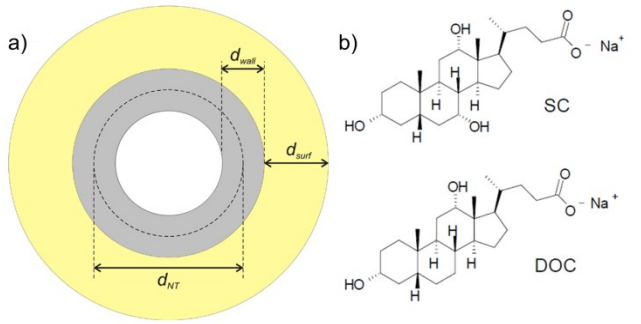

Fig. 8 a) Geometrical model of a surfactant-coated SWCNT. The SWCNT has a diameter, d_{NT}, and a wall-thickness, d_{wall}. The surfactant - hydration layer is treated as a continuous concentric cylindrical shell, and has a thickness of d_{surf}. b) Chemical structure of the SC and DOC surfactant.

From the diameter dependence of the densities of the empty SWCNTs (ρ_{int}=0), the thickness d_{surf} and the density ρ_{surf} of the surfactant – hydration layer can be obtained, by fitting the experimental data of the empty SWCNTs with equation (1). We obtain ρ_{surf}=1.1068±0.0020g/mL and d_{surf}=1.152±0.022nm for the DOC-suspended SWCNTs, and ρ_{surf}=1.1444±0.0024g/mL and d_{surf}=1.453±0.046nm for the SC sample (Section S5 in the SI discusses the error analysis for the fit parameters). Note that for the fit of the SC-suspended SWCNTs, the data points for d=1.26-1.35nm were not included as they show more complex behaviour that cannot be described by this simple model (with constant d_{surf} and ρ_{surf} for all chiralities, see below). The so-obtained fits are presented in Figure 7 (orange curves). Note also that here, the surfactant layer (characterised by d_{surf} and ρ_{surf}) is defined as the concentric cylindrical volume around the SWCNT with different density compared to the surrounding bulk solution, and includes the surfactant molecules, but also the intercalated water molecules and empty spaces, and possibly a first hydration layer from which the gradient medium may be excluded, but not the much thicker hydration layer which has the same composition and density as the surrounding bulk solution (and which therefore does not change the buoyant density in isopycnic equilibrium). This is different from the parameter definitions used in the previous sedimentation rate based AUC analyses in references [17, 18], where the entire hydration layer of correlated molecules (even if of the same density as the bulk solution) adds to the friction experienced by the sedimenting tubes, and is thus included as a separate, much thicker layer of density equal to the surrounding solution density (there set to ~1g/mL), while the surfactant layer is there defined as a much thinner equivalent volume containing only the anhydrous surfactant excluding the intercalated molecules or empty spaces between the flat SWCNT surface and surfactant molecules, based on the higher anhydrous surfactant density from literature. Thus, rate based separations yield more information on the hydration layer, while isopycnic separations yield a more precise determination of the density of the SWCNT-surfactant complex, as the density is less “diluted” by the very large hydration volume.

Secondly, the density difference between empty and water-filled SWCNTs is larger for the DOC-wrapped SWCNT compared to the SC-wrapped SWCNTs, which is in fact in agreement with the thicker surfactant layer for SC (larger V_{total}) because:

$$\rho_{filled} - \rho_{empty} = \frac{m_{D_2O}}{V_{total}} \quad \text{(eq. 2)}$$

and it can be assumed that the mass of D_2O encapsulated inside the SWCNTs is not influenced by the externally adsorbed surfactants (with m_{D2O} the mass of D_2O per unit length). This is further supported by the fact that the RBM and PLE shifts due to water-filling are nearly identical for DOC and SC-wrapped SWCNTs.

Knowing the thickness of the surfactant layer (and thus also V_{total}) determined above, we can thus extract the density

the encapsulated water, by using equation (2). Figure 9 presents the mass percentage of H_2O inside the SWCNTs (m_{H2O}/m_{CNT} ; stars and circles), obtained from the measured density difference between empty and filled SWCNTs (scaling from D_2O to H_2O was performed for easier comparison with literature data). These mass percentages are in very good agreement with predictions from molecular dynamics simulations (24-29wt% for a (10,10) SWCNT, which has a diameter of 1.38nm)[30-32], and with ensemble-averaged results from X-ray diffraction (a sample with a mean diameter of 1.41nm yielded a mass percentage of 15.5% after 100h of exposure to water vapour, but equilibrium was not yet fully reached).[33] Note that, as expected, the SC and DOC-suspended SWCNTs are found to be filled with the same amount of water (while based on very different d_{surf}), further demonstrating the consistency of the surfactant layer model.

The mass percentage of H_2O inside the SWCNTs can also be compared with a very simple model which we devised before,[13] where the water molecules are approximated by hard spheres and extrapolating the results from Picket *et al*.[29] describing the closest packing of such hard spheres inside a cylinder (blue curve in Figure 9). As before, [13] the density of the spheres was set such that the bulk close packing of spheres (as obtained in the limit of large SWCNT diameters), yields the bulk density of water. However, for the diameter of the spheres we now used the core diameter of the (5,3) SWCNT (d_{water}=0.208nm), which is the smallest diameter SWCNT in which water-filling has been experimentally observed (and which is also close to the critical diameter for filling expected theoretically).[26] Details on the hard sphere model and the obtained internal water density are given in the SI (Section S6 and Figure S10). This model is in excellent agreement with the experimental data, perfectly reproducing the overall slope of the mass percentage with diameter. This demonstrates that the filled SWCNTs are indeed entirely filled with densely packed water molecules. For comparison with the original data, we also inserted the water density of this hard-sphere model into equation 1, to obtain the density of the water-filled SWCNTs, as shown in Figure 7 (solid blue curves; note that no additional fit parameters are introduced to obtain these curves).

In addition to the general trend that is well described by the continuous model with concentric cylinders of constant d_{surf} and ρ_{surf}, the SC-wrapped SWCNTs also show pronounced oscillations in density, occurring at the same diameters for empty and filled tubes (Figure 7, d=1.26-1.35nm), which arises from the packing of the discrete (and relatively large, semi-rigid) bile salt surfactant molecules on the SWCNT surface.

Such a sudden increase in SWCNT density (for SC-dispersed SWCNTs), would indicate either a decrease of the surfactant layer thickness by up to 35% (if the density ρ_{surf} remains the same), or an increase of its density by up to 2.7% (if the thickness of the surfactant layer remains constant). Our data for the empty tubes alone is not able to discriminate between both effects or a combination of both, but they already

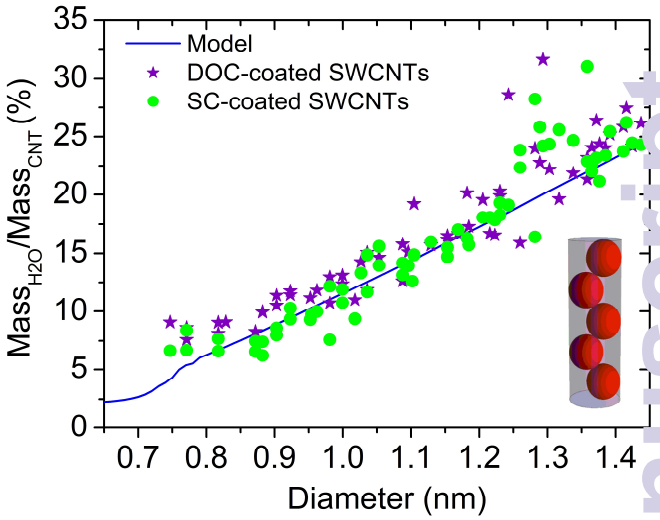

Fig. 9 Mass percentage of encapsulated water (H_2O) with respect to mass of SWCNT, s a function of diameter obtained from the experimental data for DOC-coated (purple stars) and SC-coated (green circles) SWCNTs. The blue curve represents a model w the water molecules are treated as hard spheres inside a cylinder, based on Picket *et al.* [29] as in reference [13]. The inset presents a side view of a SWCNT filled with such spheres. There is a very good agreement between the experimentally determined mass percentages and those obtained from the simple model.

indicate that for certain chiralities a different packing of the surfactant molecules results in a sudden increase in density the SWCNTs. However, the fact that the apparent mass fraction of encapsulated water in the water-filled tubes, derived from eq. 2, deviates upward for these diameter around 1.3nm (see Fig. 9), indicates that actually it is main the surfactant layer thickness (and thus V_{total} in eq. 2) which i reduced for these particular SWCNT diameters. Thes fluctuations are most pronounced for the larger diamete (d=1.26-1.35nm) SC-coated SWCNTs, but most probably als induce the small deviations in density for the smalles diameter (d<0.9nm) DOC-coated water-filled SWCNTs (Figur 7). Note that the only difference between SC and DOC is that the cholesterol group of SC bears three OH groups, all on e same side of the cholesterol group, whereas DOC has only two (see Figure 8b). The three OH groups of SC divide the flattened, semi-rigid bean shape of the cholesterol group int a polar and apolar face, so that when adsorbed on the SWCN it is very likely to adsorb with its apolar face flat onto the SWCNTs, thus creating a stacking which may or may not mat with the circumference of the SWCNTs. Only when the packing matches with the SWCNTs' circumference, a compact (high density, lower surfactant thickness) wrapping is possible, corresponding e.g. to the SWCNTs in the diameter range d=1.26-1.35nm.

In contrast, for DOC, the two OH groups create only one pola edge, which may result in other orientations on the SWCN surface, possibly tilted and partially overlapping, which wou allow for a more flexible and gradual adaptation to differe SWCNT diameters, explaining the absence of pronounce oscillations in the density-diameter relation for larger diamete DOC-coated SWCNTs. The less flexible SC-surfactant wrapp

might also lie at the origin of the stronger aggregation observed for SC-coated SWCNTs during centrifugation.

While these fluctuations in density and thus different surfactant stackings aid in separating specific chiralities, and most likely lie at the basis of the excellent separations obtained with SC for small diameter SWCNTs,[6, 10] the diameters at which they occur cannot be easily predicted. In contrast, DOC-coated SWCNTs show a more predictable density-diameter relation, becoming steeper for larger diameter empty SWCNTs, which is promising for extending the separations to larger diameters.

Conclusions

We have developed a new method to obtain rapid and very detailed chirality-dependent density-information from density gradient ultracentrifugation, by measuring full 2D PLE and RRS spectra as a function of height, directly in the centrifuge tube. We have demonstrated the importance of this method by comparing the isopycnic DGU sorting of empty and water-filled SWCNTs using two very similar surfactants, SC and DOC. The spectroscopic chirality selectivity enabling the simultaneous characterisation of a wide range of SWCNT diameters allows for deriving both surfactant layer thickness and density, in the assumption that these are constant, and moreover allows for deviations from this assumption for specific diameters to be recognized (e.g. indicating a reduced SC layer thickness for tube diameters of ~1.26-1.35nm). The speed and ability to determine surfactant layer density (which instead had to be estimated from literature data on DOC in previous AUC work[17, 18]) as well as thickness will make this technique particularly useful in systematic studies of the DGU separation parameters, in particular the choice of (co-)surfactant(s) and their concentrations, to improve the DGU separations of SWCNTs. While isopycnic separations yield high precision density measurements, rate based separations yield complementary information on the hydration layer,[17, 18] not distinguishable by density. As sedimentation rate experiments can in principle also be performed with preparative centrifuges, by characterising the centrifuge tube after different, shorter centrifugation times (till now only performed by manual extraction or visual inspection[8, 24]), one can also envisage the combination of such experiments with the present spectroscopic setup to simultaneously obtain chirality dependent information (however, for sedimentation experiments, the highest precision is still obtained on chirality- and preferably also length-sorted samples in AUC,[18] which remains time consuming). The extremely small structural difference between the two surfactant molecules, i.e. one additional hydroxylgroup for SC, has a drastic effect on the surfactant ordering around the SWCNTs, which results in qualitatively different DGU sorting behaviour. We have found that DOC-coated SWCNTs show a much smoother density-diameter relation, ascribed to a homogeneous coating that more flexibly adapts to different SWCNT diameters, in particular interesting for predictable and controllable diameter separations of larger diameter SWCNTs, while SC-coated SWCNTs show pronounced density oscillations which are interesting for separating specific chiralities.

Our results are not only important for the separation of SWCNTs by DGU, but will certainly also be useful for other separation methods that are governed by differences in the surfactant coating, such as gel chromatography[34] and the more recently introduced aqueous two-phase separation method.[35, 36]

Acknowledgements

Financial support from the Fund for Scientific Research – Flanders (FWO ; projects G040011N, G021112N and 1513513N) and the Hercules Foundation (grant AUHA/13006) is gratefully acknowledged. S.C. is a postdoctoral fellow of the FWO. The authors thank A. Herman, L. Moens and S. Dewilde for use of the Kontron ultracentrifuge.

Notes and references

1 M. A. El-Sayed, *Acc. Chem. Res.*, 2001, **34**, 257.
2 A. Jorio, M. S. Dresselhaus and G. Dresselhaus, *Carbon Nanotubes: Advanced Yopics in the Synthesis, Structure, Properties and Applications*, Springer, 2008.
3 A. H. Castro Neto, F. Guinea, N. M. R. Peres, K. S. Novoselov and A. K. Geim, *Rev. Mod. Phys.*, 2009, **81**, 109.
4 S. Iijima and T. Ichihashi, *Nature*, 1993, **363**, 603.
5 C. A. Price, *Centrifugation in Density Gradients*, Academic Press Inc, New York, 1982.
6 M. S. Arnold, A. A. Green, J. F. Hulvat, S. I. Stupp and M. C. Hersam, *Nat. Nanotechn.*, 2006, **1**, 60.
7 A. A. Green and M. C. Hersam, *Nano Lett.*, 2009, **9**, 4031.
8 O. M. Bakr, V. Amendola, C. M. Aikens, W. Wenseleers, R. Li, L. Dal Negro, G. C. Schatz and F. Stellacci, *Angew. Chem. Int. Ed.*, 2009, **121**, 6035.
9 R. P. Carney, J. Y. Kim, H. Qian, R. Jin, H. Mehenni, F. Stellacci and O. M. Bakr, *Nat. Commun.*, 2011, **2**, 335.
10 S. Ghosh, S. M. Bachilo and R. B. Weisman, *Nat. Nanotechn.*, 2010, **5**, 443.
11 J. A. Fagan, M. L. Becker, J. Chun and E. K. Hobbie, *Adv. Mater.*, 2008, **20**, 1609.
12 A. A. Green and M. C. Hersam, *Nat. Nanotechn.*, 2009, **4**, 64.
13 S. Cambré and W. Wenseleers, *Angew. Chem. - Int. Ed.*, 2011, **50**, 2764.
14 J. A. Fagan, J. Y. Huh, J. R. Simpson, J. L. Blackburn, J. M. Holt, B. A. Larsen and A. R. H. Walker, *ACS Nano*, 2011, **5**, 3943.
15 A. A. Green, M. C. Duch and M. C. Hersam, *Nano Res.*, 2009, **2**, 69.
16 J. Kang, J.-W. T. Seo, D. Alducin, A. Ponce, M. J. Yacaman and M. C. Hersam, *Nat Commun*, 2014, **5**, 5478.
17 M. S. Arnold, J. Suntivich, S. I. Stupp and M. C. Hersam, *ACS Nano*, 2008, **2**, 2291.
18 J. A. Fagan, M. Zheng, V. Rastogi, J. R. Simpson, C. Y. Khripin, C. A. S. Batista and A. R. H. Walker, *ACS Nano*, 2013, **7**, 3373.

19 W. Wenseleers, Vlasov, II, E. Goovaerts, E. D. Obraztsova, A. S. Lobach and A. Bouwen, *Adv. Funct. Mater.*, 2004, **14**, 1105.
20 F. Bonaccorso, T. Hasan, P. H. Tan, C. Sciascia, G. Privitera, G. Di Marco, P. G. Gucciardi and A. C. Ferrari, *J. Phys. Chem. C*, 2010, **114**, 17267.
21 M. J. Bronikowski, P. A. Willis, D. T. Colbert, K. A. Smith and R. E. Smalley, *J. Vac. Sci. Technol. A*, 2001, **19**, 1800.
22 C. Journet, W. K. Maser, P. Bernier, A. Loiseau, M. L. de la Chapelle, S. Lefrant, P. Deniard, R. Lee and J. E. Fischer, *Nature*, 1997, **388**, 756.
23 W. Wenseleers, S. Cambré, J. Čulin, A. Bouwen and E. Goovaerts, *Adv. Mater.*, 2007, **19**, 2274.
24 N. Nair, W.-J. Kim, R. D. Braatz and M. S. Strano, *Langmuir*, 2008, **24,** 1790.
25 S. M. Bachilo, M. S. Strano, C. Kittrell, R. H. Hauge, R. E. Smalley and R. B. Weisman, *Science*, 2002, **298**, 2361.
26 S. Cambré, B. Schoeters, S. Luyckx, E. Goovaerts and W. Wenseleers, *Phys. Rev. Lett.*, 2010, **104**, 207401.
27 S. Cambré, J. Campo, C. Beirnaert, C. Verlackt, P. Cool and W. Wenseleers, *Nat. Nanotechn.*, 2015, **10**, 248.
28 M. J. O'Connell, S. Sivaram and S. K. Doorn, *Phys. Rev. B*, 2004, **69**, 235415.
29 G. T. Pickett, M. Gross and H. Okuyama, *Phys. Rev. Lett.*, 2000, **85**, 3652.
30 A. Quintilla, F. Hennrich, S. Lebedkin, M. M. Kappes and W. Wenzel, *Phys. Chem. Chem. Phys.*, 2010, **12**.
31 A. Alexiadis and S. Kassinos, *Chem. Rev.*, 2008, **108**, 5014.
32 A. I. Kolesnikov, J.-M. Zanotti, C.-K. Loong, P. Thiyagarajan, A. P. Moravsky, R. O. Loutfy and C. J. Burnham, *Phys. Rev. Lett.*, 2004, **93**, 35503.
33 E. Paineau, P.-A. Albouy, S. Rouzière, A. Orecchini, S. Rols and P. Launois, *Nano Lett.*, 2013, **13**, 1751.
34 H. Liu, D. Nishide, T. Tanaka and H. Kataura, *Nat. Commun.*, 2011, **2**, 309.
35 J. A. Fagan, C. Y. Khripin, C. A. Silvera Batista, J. R. Simpson, E. H. Hároz, A. R. Hight Walker and M. Zheng, *Adv. Mater.*, 2014, **26**, 2800.
36 N. K. Subbaiyan, S. Cambré, A. N. G. Parra-Vasquez, E. H. Hároz, S. K. Doorn and J. G. Duque, *ACS Nano*, 2014, **8**, 1619.